Wavelet-Based Islanding Detection in Grid-Connected PV Systems

Alberto Pigazo, *Member, IEEE*, Marco Liserre, *Senior Member, IEEE*, Rosa A. Mastromauro, *Member, IEEE*, Víctor M. Moreno, *Member, IEEE*, and Antonio Dell'Aquila, *Member, IEEE*

***Abstract*—Distributed power generation systems (DPGSs) based on inverters require reliable islanding detection algorithms (passive or active) in order to determine the electrical grid status and operate the grid-connected inverter properly. These methods are based on the analysis of the DPGS voltage, current, and power in time or frequency domain. This paper proposes a time–frequency detection algorithm based on monitoring the DPGS output power considering the influence of the pulsewidth modulation, the output LCL filter, and the employed current controller. Wavelet analysis is applied to obtain time localization of the islanding condition. Simulation and experimental results show the performance of the proposed detection algorithm in comparison with existing methods.**

***Index Terms*—Islanding, photovoltaic (PV) power systems, wavelet transforms.**

I. Introduction

A MAIN ISSUE associated with renewable energy sources connected to electrical grids through an active front end is the proper operation of such grid interfaces in order to improve the power supply reliability and quality independently from the electrical characteristics of the renewable energy source and the grid conditions at the point of common coupling (PCC) [1]–[4]. The power converter topology [5]–[7], the controller structure, the supported functionalities, and/or implementation issues [8] must be considered during the design process of the active front end; however, according to international standards [9]–[16], the detection of the islanding condition must be also considered.

The islanding condition is defined in [9] and occurs when "a portion of the utility system that contains both load and distributed resources remains energized while it is isolated from the remainder of the utility system." In case of low-power *plug&play* photovoltaic (PV) systems, according to [13], the distributed resource must be stopped within 2 s of the formation of the unintentional island in order to avoid possible damages to local electrical loads or the PV inverter during the grid reconnection. Moreover, this condition can be mandatory in order to guarantee the safety of workers during maintenance operations of the electrical system [17].

The detection of the islanding condition is a classical issue in electrical engineering; however, it must be considered that in low-power PV distributed power generation systems (DPGSs), where a minimum number of sensors is required to reduce the economical costs or, simply, load- and grid-side sensors are not available, this condition must be determined from voltage and current measurements at the inverter side of the PCC [18]. Wireless communication systems have decreased their cost and can be an alternative in future DPGSs. Passive, active, and hybrid detection methods have been proposed in the literature as alternatives to grid-level detection methods.

Passive methods monitor the voltage and current at the inverter side of the PCC. Measurements of the PCC voltage magnitude and frequency [19], [20], harmonics [21], and phase [22] are considered, separately or simultaneously [23], in order to determine the islanding condition [24]. As a drawback, it must be considered that the proper operation of passive methods under all possible load, grid, and DPGS powers cannot be guaranteed [25]. The nondetection zone (NDZ) of each method [26] can be calculated in order to evaluate the detection techniques [27]. Moreover, it must be considered that grid voltage disturbances can cause the inopportune intervention of the antiislanding algorithm during normal operation.

Active detection methods have been introduced as an alternative to passive methods. In this case, a controlled disturbance is introduced at the PCC, and when the islanding condition occurs, the disturbance forces the detection method threshold [28], [29], and as a consequence, the NDZ is minimized or avoided. Diverse methods, such as impedance measurement or detection [30]–[32], slip-mode frequency shifting (SMS) [33], active and reactive power variations [34], and active frequency drift [35], have been proposed; however, as drawbacks, they introduce a disturbance at the PCC, and interaction between DPGSs must be considered [36]. Hybrid methods combine the effectiveness of passive and active approaches and can be applied as an alternative [37].

This paper extends the analysis given in [38] and proposes a wavelet-based detection method which can detect the islanding condition from the local measurements of PCC voltage and current signals, as in case of passive methods, but evaluates the high-frequency components injected by the PV inverter, which depend on the characteristics of the employed pulsewidth modulator, LCL filter, and current controller, to reveal the islanding condition, as done by active methods. As it will be

Manuscript received October 31, 2007; revised June 13, 2008. First published July 9, 2008; current version published October 9, 2009. This paper was supported in part by the Spanish Ministry of Science and Innovation under Grant ENE2007-63979/ALT.

A. Pigazo and V. M. Moreno are with the Department of Electronics and Computers, University of Cantabria, 39005 Santander, Spain (e-mail: pigazoa@unican.es; morenov@unican.es).

M. Liserre, R. A. Mastromauro, and A. Dell'Aquila are with the Department of Electrical and Electronics Engineering, Politecnico di Bari, 70126 Bari, Italy (e-mail: liserre@ieee.org; mastromauro@deemail.poliba.it; dellaqui@poliba.it).

Digital Object Identifier 10.1109/TIE.2008.928097

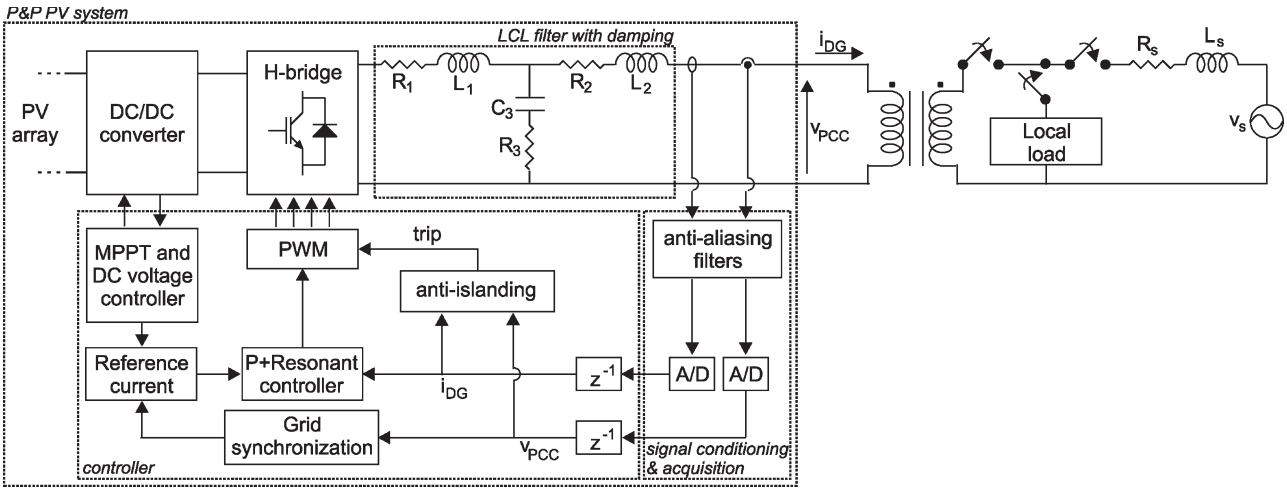

Fig. 1. Grid interface of the "plug&play" PV system under test according to IEEE Std. 1547.1 [14].

shown, the spectrum of the PV inverter output power will suffer a small variation after the islanding operation mode over a continuous and relatively wide frequency band. Passive harmonic detection (HD) methods based on discrete Fourier transform do not allow these variations to be detected due to their low resolution, which depends on the number of selected harmonics. As a consequence, wavelet filter banks are proposed for tracking purposes of such spectrum variations in a properly selected frequency band. Section II shows the basis of the proposed method, including the procedure for the selection of a suitable mother wavelet. Section III describes the selection method of proper detection levels and gives the NDZ of the proposed method and a comparison of two conventional detection methods. Sections IV and V present the obtained experimental results and conclusions, respectively.

II. Proposed Detection Method

The structure of a conventional inverter-based PV system is analyzed in this section. Special attention is given to the high-frequency behavior of the inverter output signals (voltage, current, and power) and the impact of the PV inverter characteristics on these signals. This is the basis for proposing an antiislanding detection method using wavelet analysis and a methodology for the proper selection of a mother wavelet for islanding detection purposes.

A. Grid Interface of Single-Phase PV System

The general structure of a grid-connected PV system is shown in Fig. 1. The dc/dc stage operates using a perturb-and-observe algorithm that adapts the voltage of the PV array in order to track the maximum power point (MPP) as temperature and irradiation change. Hence, the MPP tracking (MPPT) computes the power that will be injected into the grid, whereas the dc voltage controller adjusts it in order to keep the dc voltage constant at the input of the H-bridge. Both MPPT and dc voltage controller contribute to determine the reference current, as shown in Fig. 1. The characteristics of the employed MPPT algorithm must be considered in order to evaluate the performance of the overall PV systems [39]; however, due to the presence of the dc/dc converter, its impact on the performance of the anti-islanding algorithm can be neglected. The H-bridge is a full bridge. The ac peak voltage is 325 V. This voltage could be 15% higher [9]–[15]; the grid filter can add a 10% voltage drop, and hence, the ac voltage generated by the ac converter should be at least 406 V. Industrial inverters adopt a dc voltage 20%–50% higher than this value in order to have a safety margin. A signal conditioning and acquisition stage allows the output current i_{DG} and the PCC voltage v_{pcc} to be measured. A low-pass filter (LPF) is employed in order to avoid the aliasing effect associated with the acquisition of high-frequency components in i_{DG} and v_{pcc} signals. The controller establishes the switching states of the grid-connected current-controlled single-phase inverter through a pulsewidth modulator. Sideband harmonics of the modulator carrier signal are minimized by introducing a properly designed LCL filtering stage [40]. The current controller is made by a proportional component and by a resonant term at the grid frequency. Details about the design process of this kind of controllers can be found in [41]. Three switches connected to the PCC allow islanding tests to be carried out according to IEEE Std. 1547.1 [14]. A test resonant load (R_{L}, C_{L}, and L_{L}), with a quality factor of 1.25, has been considered during the islanding tests, both in simulation and in experiment, due to the laboratory restrictions. It must be considered that IEEE Std. 1547.1 suggests a quality factor equal to one [14].

Fig. 2 shows a simplified scheme, where the DPGS inverter has been modeled as a voltage source v_{DG} operating with multiple frequencies which depend on the employed pulsewidth modulation technique [42]. The LCL filter (R_1, L_1, R_2, L_2, R_3, and C_3) has been modeled considering ideal passive elements; R_{s} and L_{s} allow the effect of the grid impedance to be considered, and the nonintentional islanding operation can be simulated by means of the switch sw. It must be considered that once the islanding condition occurs, v_{DG} can suffer variations due to the dynamic characteristics of the grid synchronization algorithm included in the PV inverter controller.

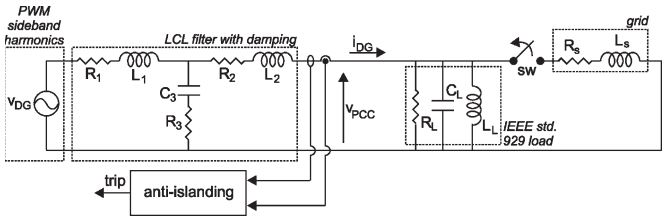

Fig. 2. Schematic of the high-frequency equivalent circuit.

TABLE I
PARAMETERS OF ANALYZED PV SYSTEM

Parameter	Value	Parameter	Value
R_1, R_2	$0.5\ \Omega$	R_3	$5\ \Omega$
L_1	$3\ mH$	L_2	$1\ mH$
C_3	$5\ \mu F$	C_L	$37.6\ \mu F$
R_L	$105.8\ \Omega$	L_L	$269.4\ mH$
L_s	$2\ mH$	R_s	$0.5\ \Omega$
V_{dc}	$600\ V$	$f_{carrier}$	$6.4\ kHz$
P_{load}	$500\ W$	Q_{load}	$0\ VA$

B. Frequency Behavior of Equivalent High-Frequency PV System and Basis of Proposed Method

The frequency spectra of the output current $i_{\rm DG}$, the PCC voltage $v_{\rm pcc}$, and the instantaneous output power $p_{\rm DG}$ signals have been measured through a simulation model matching the structure shown in Fig. 1. The grid interface of the PV system has been analyzed both in grid-connected and islanding operation modes. Table I shows the employed simulation parameters, which correspond to the worst case for passive antiislanding detection methods ($P_{\rm DG} = P_{\rm load}$ and $Q_{\rm DG} = Q_{\rm load}$). The employed antialiasing filters are second-order LPFs with $f_{\rm carrier}/4$ cutoff frequencies. The LCL filter has been designed considering that the 1Φ DPGS inverter is controlled by means of a pulsewidth modulator which takes advantage of the unipolar modulation to reduce the weighted total harmonic distortion (THD) of $i_{\rm DG}$ [42]. The dc-bus voltage has been established at 600 V in order to ensure an appropriate current injection at the PCC through the LCL filter; however, in practical PV systems, this value should be properly adjusted in order to improve the overall performance.

The spectra of the measured signals without the fundamental component are shown in Fig. 3. The employed base values are $V_{\rm base} = 230$ V, $I_{\rm base} = 3.33$ A, and $P_{\rm base} = P_{\rm load}$. Considering the PCC voltage, the inverter does not deteriorate the quality of the voltage waveform during the grid-connected operation, a 0.12% voltage (VTHD); however, during the islanding operation, the distortion of the PCC voltage increases up to 0.19% [Fig. 3(a)]. As shown in Fig. 3(b), the LCL filter attenuates the sideband harmonics of the pulsewidth modulator during the grid-connected operation, and the THD of the $i_{\rm DG}$ signal is low (1.94%) and within the limits established by IEEE Std. 929 [9]. The current THD (ITHD) increases during the islanding operation mode, reaching 3.52%. The instantaneous output power $p_{\rm DG}$ consumption in a grid-connected mode is carried out at the fundamental grid frequency; however, during the islanding operation mode, other frequencies appear due to harmonics [Fig. 3(c)].

The dependence of $v_{\rm pcc}$, $i_{\rm DG}$, and $p_{\rm DG}$ on $v_{\rm DG}$ during each possible operation mode at high frequency can be analyzed

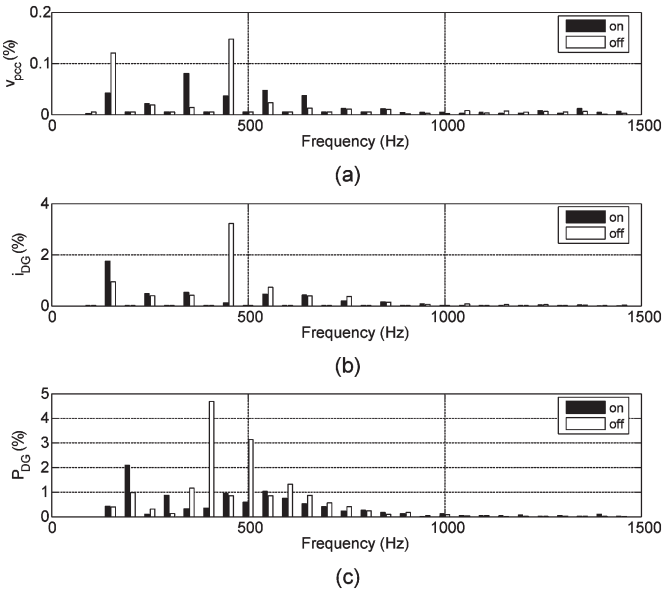

Fig. 3. Spectra of (a) PCC voltage, (b) DPGS output current, and (c) DPGS output power in grid-connected and disconnected operations.

mathematically, considering the circuit model shown in Fig. 2. Due to the developed analysis, the effects of possible $V_{\rm DG}$ changes during the grid-disconnection transient are neglected. From the complex impedances in Fig. 2

$$Z_1(j\omega_{\rm DG}) = R_1 + j\omega_{\rm DG}L_1 \tag{1}$$
$$Z_2(j\omega_{\rm DG}) = R_2 + j\omega_{\rm DG}L_2 \tag{2}$$
$$Z_3(j\omega_{\rm DG}) = \frac{j\omega_{\rm DG}R_3C_3 + 1}{j\omega_{\rm DG}C_3} \tag{3}$$
$$Z_{\rm L}(j\omega_{\rm DG}) = R_{\rm L}//\frac{1}{j\omega_{\rm DG}C_{\rm L}}//j\omega_{\rm DG}L_{\rm L} \tag{4}$$
$$Z_{\rm S}(j\omega_{\rm DG}) = R_{\rm S} + j\omega_{\rm DG}L_{\rm S} \tag{5}$$

result

$$V_{\rm pcc} = V_{\rm DG}\frac{Z_3(Z_{\rm L}//Z_{\rm S})}{Z_1Z_2 + Z_1Z_3 + Z_2Z_3 + (Z_1 + Z_3)Z_{\rm L}//Z_{\rm S}} \tag{6}$$
$$I_{\rm DG} = \frac{V_{\rm pcc}}{Z_{\rm L}//Z_{\rm S}} \tag{7}$$
$$P_{\rm DG} = \frac{V_{\rm pcc}^2}{Z_{\rm L}//Z_{\rm S}} \tag{8}$$

where $P_{\rm DG}$ is the frequency domain representation of the output power of the PV system corresponding to the baseband harmonics of the PWM carrier signal. Hence, the dependence of each magnitude from the DPGS voltage at each output frequency different from the fundamental component can be evaluated by means of

$$\left|\frac{\partial V_{\rm pcc}}{\partial V_{\rm DG}}\right|_{\rm on} = \left|\frac{Z_3(Z_{\rm L}//Z_{\rm S})}{Z_1Z_2 + Z_1Z_3 + Z_2Z_3 + (Z_1 + Z_3)Z_{\rm L}//Z_{\rm S}}\right| \tag{9}$$
$$\left|\frac{\partial I_{\rm DG}}{\partial V_{\rm DG}}\right|_{\rm on} = \left|\frac{1}{Z_{\rm L}//Z_{\rm S}}\right|\left|\frac{\partial V_{\rm pcc}}{\partial V_{\rm DG}}\right|_{\rm on} \tag{10}$$
$$\left|\frac{\partial P_{\rm DG}}{\partial V_{\rm DG}}\right|_{\rm on} = \left|\frac{2V_{\rm DG}}{Z_{\rm L}//Z_{\rm S}}\right|\left|\frac{\partial V_{\rm pcc}}{\partial V_{\rm DG}}\right|_{\rm on}^2 \tag{11}$$

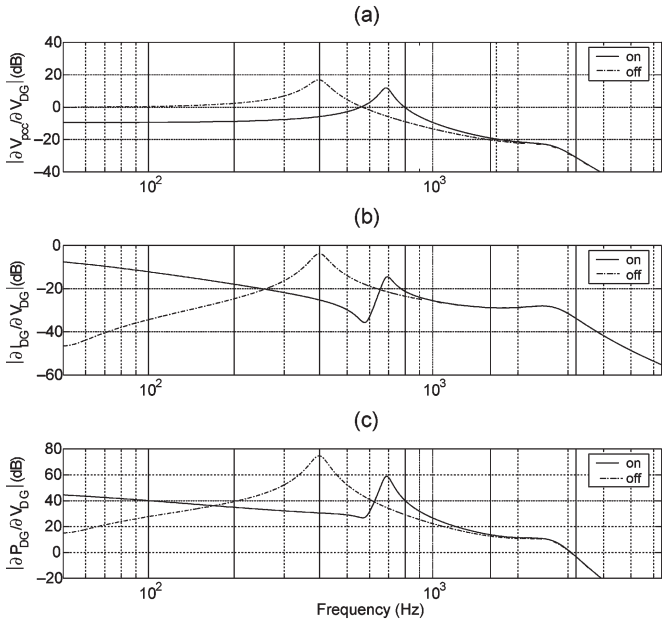

Fig. 4. Frequency response of the equivalent circuit at high frequency when the DPGS inverter is connected (on) and when it is not connected (off) to the grid.

where the subindex on denotes a grid-connected operation. In order to minimize the effect of high-frequency components of the PV system on the PCC voltage and current signals, the output LCL filter, Z_1, Z_2, and Z_3 must be properly designed [40]. The islanding operation mode can be analyzed by switching sw, and hence, (9)–(11) can be rewritten as

$$\left|\frac{\partial V_{\rm pcc}}{\partial V_{\rm DG}}\right|_{\rm off} = \left|\frac{Z_3(Z_{\rm L})}{Z_1Z_2 + Z_1Z_3 + Z_2Z_3 + (Z_1+Z_3)Z_{\rm L}}\right| \quad (12)$$

$$\left|\frac{\partial I_{\rm DG}}{\partial V_{\rm DG}}\right|_{\rm off} = \left|\frac{1}{Z_{\rm L}}\right| \left|\frac{\partial V_{\rm pcc}}{\partial V_{\rm DG}}\right|_{\rm off} \quad (13)$$

$$\left|\frac{\partial P_{\rm DG}}{\partial V_{\rm DG}}\right|_{\rm off} = \left|\frac{2V_{\rm DG}}{Z_{\rm L}}\right| \left|\frac{\partial V_{\rm pcc}}{\partial V_{\rm DG}}\right|^2_{\rm off}. \quad (14)$$

The frequency responses of (9)–(14) considering a conventional single-phase PV DPGSs parameterized in Table I are shown in Fig. 4. As shown in Fig. 4(a), the dependence of the PCC voltage on the DPGS output voltage during a grid-connected operation is low; however, once the islanding condition occurs, the PCC voltage is controlled by the DPGS inverter output voltage. The difference between gains reaches 22.76 dB at 395.3 Hz. If the output current $I_{\rm DG}$ is considered [Fig. 4(b)], the difference reaches 37 dB at 48.44 Hz. Finally, analyzing the dependence of the DG output power $P_{\rm DG}$ from $V_{\rm DG}$ [Fig. 4(c)], a difference of 44 dB is reached at 398.44 Hz. Hence, the greatest gain difference is reached considering (11) and (14).

Based on the obtained results, the islanding-mode operation can be detected by measuring the amplitude variation of certain frequencies of the measured spectra ($|\partial V_{\rm pcc}/\partial V_{\rm DG}|$, $|\partial I_{\rm DG}/\partial V_{\rm DG}|, |\partial P_{\rm DG}/\partial V_{\rm DG}|$). Depending on the number of resonant blocks, their frequency, and the characteristics of the designed LCL filter, the frequencies which must be measured and the magnitude of the amplitude variations can be modified.

An operator MA$(f_{\rm s}, f_{\rm e}, S)$, where $f_{\rm s}$ and $f_{\rm e}$ are the starting and ending frequencies of the considered band, respectively, and S is the frequency spectrum of the considered output signal ($v_{\rm pcc}$, $i_{\rm DG}$, or $p_{\rm DG}$), can be defined in order to determine the most appropriate frequency band and power signal for anti-islanding detection purposes

$$\mathrm{MA}(f_{\rm s}, f_{\rm e}, S) = \int_{f_{\rm s}}^{f_{\rm e}} \left(\left|\frac{\partial S}{\partial V_{\rm DG}}\right|_{\rm off} - \left|\frac{\partial S}{\partial V_{\rm DG}}\right|_{\rm on} \right) df. \quad (15)$$

Applying this operator to the frequency bands and the power signals shown in Fig. 4, the results shown in Table II are obtained. Due to the fact that a higher value of MA implies a better resolution between both grid-connected and islanding operation modes, the most appropriate output frequency bands in order to detect the islanding operation mode are the fourth and the fifth. Moreover, the values in bold allows the best values for each output signal to be compared, and hence, $P_{\rm DG}$ has been selected for detection purposes. As a consequence, applying MA to the instantaneous output power of the PV system at the fourth and the fifth frequency bands, the islanding condition could be determined. However, time localization cannot be achieved by applying (15).

C. Effects of Grid Impedance on PV System Frequency Response

Based on (9)–(11), changes in the grid impedance would change the resolution at each frequency band, and as a consequence, the performance of the proposed method could deteriorate. In order to analyze the impact of such grid impedance variations, Table II has been recalculated for 50% resistive and/or inductive variations. The obtained results, plotted as percentage of the nominal values (Table I), are shown in Fig. 5 for the fourth and the fifth frequency bands. As can be seen, the effect of the resistive variations (ΔR) is higher than the inductive ones, and their impact depends on the analyzed output signal and frequency band.

Fig. 5(a) and (b) shows the relative variation of the output of operator MA applied to $V_{\rm pcc}$ for the fourth and the fifth frequency bands, respectively. The maximum measured variations are 662.2% and 33.7%, respectively. In case of $I_{\rm DG}$ [Fig. 5(c) and (d)], the maximum variation is obtained at the fifth frequency band (40.9%), whereas the fourth frequency band output remains below 33.3%. The best measured results are obtained in case of $P_{\rm DG}$ at the fifth frequency band, with a maximum variation of 13.5% [Fig. 5(f)], whereas the measured value at the fourth frequency band is 166.2% [Fig. 5(e)].

From the analysis carried out up to this point and applied to the PV system shown in Fig. 1, it can be established that the proposed antiislanding detection method must track the fifth frequency band in order to obtain the best possible resolution and independence from the characteristics of the PCC (grid impedance). However, the IEEE Std. 1547.1 [14] establishes that the islanding condition must be detected in less than 2 s, which cannot be directly satisfied by applying (15) to the instantaneous output power of the PV inverter.

TABLE II
RESULTS OF MA(f_s, f_e, S) APPLIED TO FIG. 4

Frequency band	1^{st} $f_e = 6400\ Hz$ $f_s = 3200\ Hz$	2^{nd} $f_e = 3200\ Hz$ $f_s = 1600\ Hz$	3^{th} $f_e = 1600\ Hz$ $f_s = 800\ Hz$	4^{th} $f_e = 800\ Hz$ $f_s = 400\ Hz$	5^{th} $f_e = 400\ Hz$ $f_s = 200\ Hz$	6^{th} $f_e = 200\ Hz$ $f_s = 100\ Hz$	7^{th} $f_e = 100\ Hz$ $f_s = 50\ Hz$
$MA(V_{pcc})$	-482.9 $dB \cdot Hz$	-910.9 $dB \cdot Hz$	-2401.1 $dB \cdot Hz$	-530.5 $dB \cdot Hz$	**3087.4** $dB \cdot Hz$	974.9 $dB \cdot Hz$	404.3$dB \cdot Hz$
$MA(I_{DG})$	-23.3 $dB \cdot Hz$	37.7 $dB \cdot Hz$	-224.0 $dB \cdot Hz$	**3033.7** $dB \cdot Hz$	1282.4 $dB \cdot Hz$	-1344.6 $dB \cdot Hz$	-1448.0 $dB \cdot Hz$
$MA(P_{DG})$	-506.2 $dB \cdot Hz$	-873.2 $dB \cdot Hz$	-2625.0 $dB \cdot Hz$	2503.2 $dB \cdot Hz$	**4369.9** $dB \cdot Hz$	-369.7 $dB \cdot Hz$	-1043.7$dB \cdot Hz$

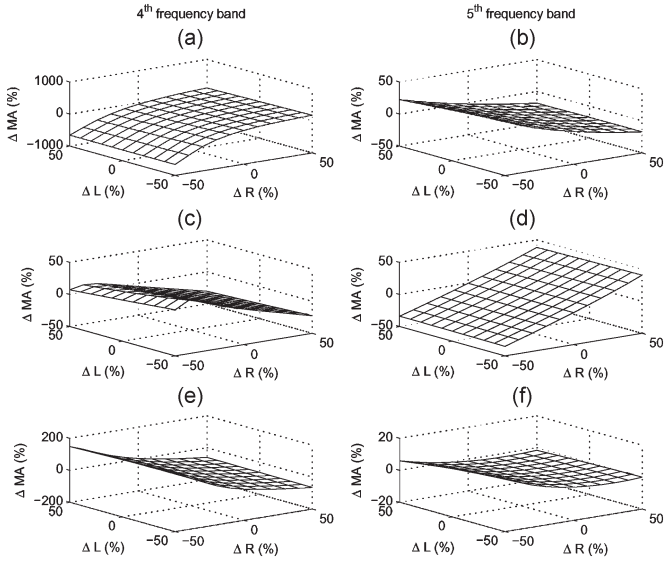

Fig. 5. Effect of grid impedance variations on islanding detection. (a) Fourth frequency band and $V_{\rm pcc}$. (b) Fifth frequency band and $V_{\rm pcc}$. (c) Fourth frequency band and $I_{\rm DG}$. (d) Fifth frequency band and $I_{\rm DG}$. (e) Fourth frequency band and $P_{\rm DG}$. (f) Fifth frequency band and $P_{\rm DG}$.

D. Wavelet Analysis Applied to Detection of Islanding Condition in Single-Phase Inverter-Based PV DPGSs

In order to accomplish the time requirements in [14], applying the wavelet analysis to obtain time localization and tracking of a certain frequency band is proposed.

The discrete wavelet transform (DWT) is a signal-processing tool which can be applied when time-varying harmonics must be evaluated [43] and, as in the case of the detection of the islanding condition, time localization is required [44]. The DWT of a discrete function $x(k)$ can be defined as

$$\mathrm{DWT}(m,k) = \frac{1}{\sqrt{a_o^m}} \sum_n x(n)\psi\left(\frac{k - n a_o^m}{a_o^m}\right) \qquad (16)$$

where m and n are positive integers employed to define scaling and translating factors applied to the selected mother wavelet ψ. Due to the possible values of m, the frequency bands which can be measured by applying the DWT are logarithmic. These bands match the ones shown in Fig. 4. From Fig. 4 and depending on the LCL-filter characteristics, the most suitable scale for islanding detection purposes can be selected. It must be considered that the response time of the antiislanding detection algorithm will be shorter if a lower decomposition level is selected [45]. As a consequence, both the fourth and the fifth decomposition levels have been selected. The selection of the most appropriate mother wavelet is a key issue when applying the wavelet analysis, and it will be discussed in the following sections.

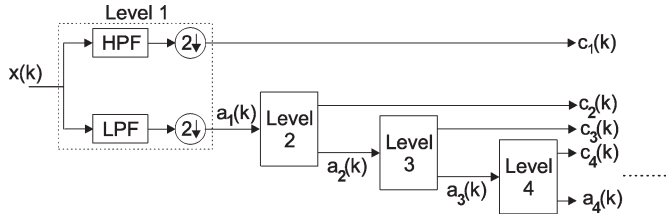

Fig. 6. Wavelet filter bank structure.

In order to simplify the detection algorithm implementation and tracking of the required frequency band, a filter bank structure, which is shown in Fig. 6, has been selected [46]. The basic functional block corresponding to each decomposition level l is implemented by means of a high-pass filter $H(z)$, which generates the decomposition *details*, and an LPF $G(z)$, whose output corresponds to the decomposition *approximation*. The downsampling stages applied to the outputs of $H(z)$ and $G(z)$ are required in order to avoid information redundancy and obtain $c_l(k)$ and $a_l(k)$. It must be considered that the coefficients of $H(z)$ and $G(z)$ depend on the selected mother wavelet ψ and the logarithmic resolution required to establish the method frequency bands are due to the dyadic downsampling blocks. From the structure shown in Fig. 6, it is clear that the computational burden depends on the number of applied decomposition levels.

E. Mother Wavelet Selection

The performance of the proposed anti-islanding detection method relies on the selection of an appropriate mother wavelet ψ. One hundred thirteen mother wavelets corresponding to Daubechies, Symlets, Coiflets, Biorthogonal, and Reverse Biorthogonal families have been tested on a simulation model corresponding to Fig. 1 and considering the worst detection conditions ($\Delta P = \Delta Q = 0$). The wavelet filter bank structure shown in Fig. 6 has been applied to the instantaneous output power of the PV inverter. The variation of the signal *details* before and after the beginning of the islanding operation at the fifth decomposition level (Δc_5) has been shown in Fig. 7 in order to determine the mother wavelet with the best resolution. Pure sinusoidal and harmonically distorted grid voltages, according to IEEE Std. 519 [first, 100%; third, 2%; fifth, 2%; and seventh, 4% (with VTHD $< 5\%$)], have been applied to the simulation model.

From the obtained results at the fifth decomposition level, the islanding operation mode is revealed in less than 2 s (IEEE Std. 1547.1) with both pure sinusoidal and distorted grid voltages. In case of sinusoidal grid voltages [Fig. 7(a)], the average value of Δc_5 for the set of analyzed mother wavelets is 3852, whereas in case of harmonically distorted grid voltages

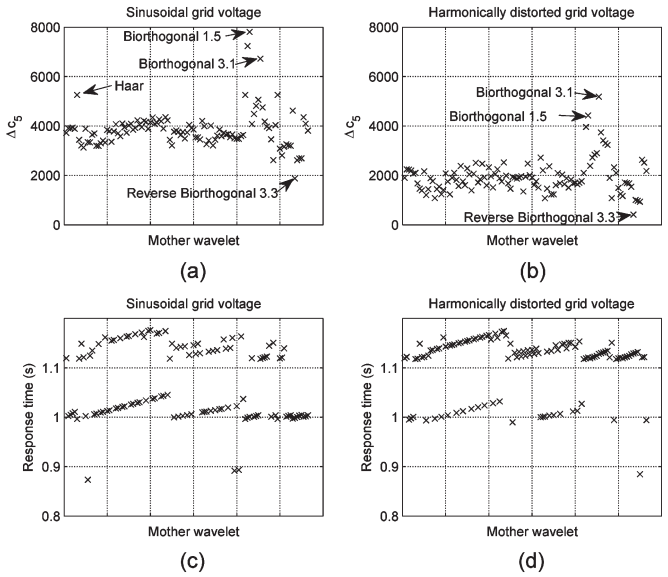

Fig. 7. Fifth decomposition level ($\Delta P = \Delta Q = 0$). *Detail* variations with (a) pure sinusoidal and (b) harmonically distorted grid voltages. (c) and (d) Measured response times.

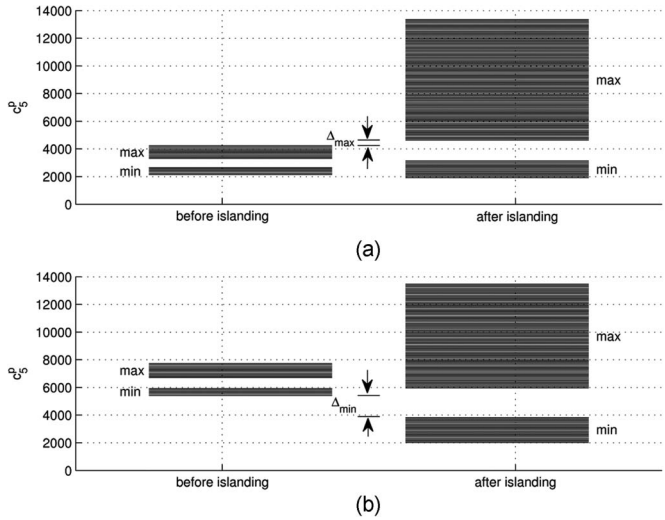

Fig. 8. Measured values of c_5^p inside the NDZ of passive methods for (a) pure sinusoidal and (b) harmonically distorted grid voltages. $\Delta_{\max} = 399$, and $\Delta_{\min} = 1534$.

[Fig. 7(b)], this value reaches only 1945.9. From Fig. 7(a), the mother wavelets with best resolutions are Biorthogonal 1.5 and 3.1, which reach $\Delta c_5 = 7809$ and 6721 with response times [Fig. 7(c)] equal to $T_{\rm r} = 0.8931$ s and $T_{\rm r} = 1.118$ s, respectively. Due to its implementation simplicity and the obtained results in case of sinusoidal PCC voltages, the Haar wavelet can be also considered as a good alternative ($\Delta c_5 = 5257$ and $T_{\rm r} = 0.9966$ s). It must be considered that the measured response times correspond to the time intervals between the beginning of the islanding operation mode and the maximum measured variation of c_5, and as a consequence, the detection times can be improved by a proper selection of tripping levels. Equivalent results are obtained in case of harmonically distorted grid voltages, Biorthogonal 1.5 and 3.1 being the best choices with $\Delta c_5 = 4420$ and $\Delta c_5 = 5183$ resolutions [Fig. 7(b)] and 1.119 and 1.128 s as the response times [Fig. 7(d)], respectively. Considering the response times and the obtained resolution levels, Biorthogonal 1.5 has been selected for the implementation of the proposed antiislanding detection algorithm.

F. Selection of Detection Levels

Once the most appropriate mother wavelet has been selected, the islanding condition can be detected by the comparison of the measured peak values of c_5 and certain detection levels previously defined. As a consequence, a peak detector must be applied to c_5 of each grid fundamental period

$$c_5^p(k) = \max\left(|c_5(k)|, \ldots |c_5(k-N+1)|\right) \qquad (17)$$

with N being the number of considered samples at the fundamental grid frequency. The measured values shown in Fig. 8 has been obtained by applying (17) to the output of the wavelet filter bank structure and considering different output powers of the PV DPGSs around $P_{\rm load}$ and $Q_{\rm load}$ (the applied maximum active and reactive power variations are 5% of the load power with 1% steps). As can be seen, due to the employed ΔP and ΔQ, the maximum and minimum values of c_5^p before and after the islanding condition describe two bands whose characteristics depend on the employed LCL filter and the switching frequency of the PV inverter. It must be considered that the shown values of c_5^p after the islanding condition correspond to the measured values of c_5^p during the transient after the grid disconnection. The bands overlap once the steady state is reached again.

The measured bands in case of pure sinusoidal PCC voltages are shown in Fig. 8(a). As can be seen and considering the minimum measured values of c_5^p, the measured values before the islanding operation are inside the band obtained after the islanding condition; however, in case of the maximum measured values, there is a distance $\Delta_{\max} = 399$ between bands which allows for reliable detection after a rising crossing of a properly selected trip level $T^{\rm H}$. In this case, the trip level has been established by adding $\Delta_{\max}/2$ to the maximum measured value before the islanding operation.

The distribution of the measured maximum and minimum values of c_5^p changes in case of harmonically distorted grid voltages according to IEEE Std. 519 [Fig. 8(b)]. In this case, the maximum measured values of c_5^p before the islanding condition are inside the measured band after the operation in an electrical island; however, the minimum values present a gap equal to $\Delta_{\min} = 1534$. From these results, a reliable detection of the islanding condition requires the comparison of the values obtained by applying (17) and two detection levels corresponding to sinusoidal and harmonically distorted grid voltages, which are $T^{\rm H}$ and $T^{\rm L}$, respectively. The PV inverter must be stopped if a raising crossing of $T^{\rm H}$ or a falling crossing of $T^{\rm L}$ occurs.

III. Simulation Results

The general structure shown in Fig. 1 has been modeled and tested by means of MatLab/Simulink and the Power Systems BlockSet. The employed parameters have been shown in Table I; the selected mother wavelet is a Biorthogonal 1.5, and

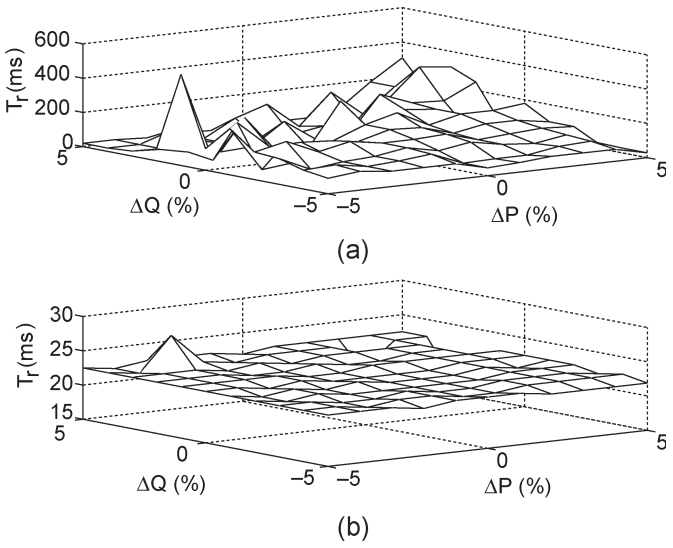

Fig. 9. Simulation results in case of (a) pure sinusoidal and (b) harmonically distorted grid voltages. $T^{\mathrm{H}} = 4440$, and $T^{\mathrm{L}} = 4655$.

the employed detection levels are $T^{\mathrm{H}} = 4440$ and $T^{\mathrm{L}} = 4655$. The designed antiislanding detection method has been tested using pure sinusoidal and distorted grid voltages.

A. NDZ of Proposed Method

The NDZ of the proposed method has been evaluated by applying the designed detection levels to the simulation model through c_5^p. The measured response times vary from half cycle at the fundamental grid frequency to 30 cycles [Fig. 9(a)] and within the range of 17.19–26.87 ms [Fig. 9(b)] in case of pure sinusoidal and harmonically distorted grid voltages, respectively. As a consequence, the islanding condition is properly detected according to [14] in both cases.

B. Performance Comparison

The proposed wavelet-based detection technique has been compared to the HD [21] and SMS [35] methods in order to evaluate their performances. The methods have been analyzed by simulation and implemented according to the general structure shown in Fig. 1.

The HD technique is a passive method which measures the THD of i_{DG} during the islanding test. Fig. 10(a) shows the obtained results in case of a pure sinusoidal grid voltage. As can be seen, the ITHD varies between 1.45% in case of grid-connected operation and a maximum 3.59% measured at $t = 1.12$ s. In order to detect the islanding condition, the detection level should be established within this range. Fig. 10(b) shows the obtained results in case of harmonically distorted grid voltages. The THD varies within 3.61%–4.39% during grid-connected operation and falls to 1.50% after the islanding condition. Hence, the measured THD before the occurrence of the islanding condition depends on the harmonic distortion of the PCC voltage. Moreover, the obtained ITHD values have a ripple which reduces the method resolution. As a consequence, a reliable detection level for all possible operation conditions and local loads cannot be properly selected. The proposed

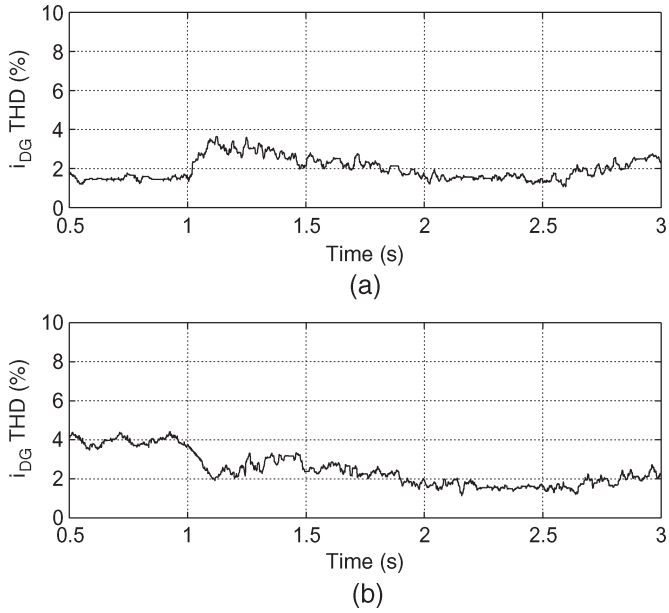

Fig. 10. HD method. THD of i_{DG} with $P_{\mathrm{DG}} = P_{\mathrm{load}}$, $Q_{\mathrm{DG}} = Q_{\mathrm{load}}$. (a) Pure sinusoidal grid voltage. (b) Distorted grid voltage. The islanding operation occurs at $t = 1$ s.

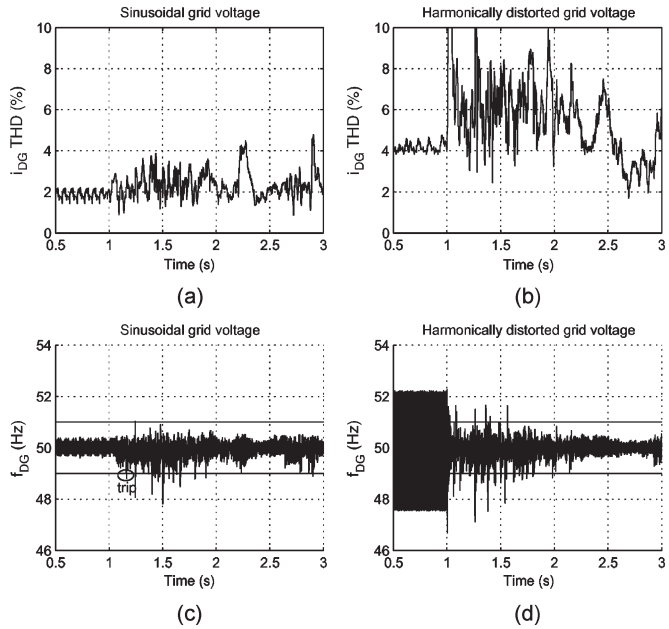

Fig. 11. SMS method with $P_{\mathrm{DG}} = P_{\mathrm{load}}$, $Q_{\mathrm{DG}} = Q_{\mathrm{load}}$. i_{DG}THD with (a) pure sinusoidal and (b) harmonically distorted grid voltages. Measured frequency at the PCC (f_{DG}) in case of (c) pure sinusoidal and (d) harmonically distorted grid voltages. The islanding condition is applied at $t = 1$ s.

wavelet-based method allows for reliable detection during all possible operation conditions (Fig. 8) by selecting the most suitable frequency band for detection purposes. Moreover, from Fig. 4, the resolution of the proposed method could be only reached by the HD technique by tracking all the harmonics inside the selected frequency band, which would increase the computational burden of the overall PV system controller.

In case of the SMS method, the phase angle of i_{DG} is dynamically changed depending on the measured mains frequency f_{DG}. Fig. 11(a) and (c) shows the measured ITHD and f_{DG}

in case of a pure sinusoidal grid voltage. f_{DG} is measured through the applied software phase-locked loop (SPLL) for synchronization purposes (Fig. 1) and, as shown in Fig. 11(c), during the grid-connected operation, is maintained within 49.61–50.37 Hz. Once the islanding occurs, the positive feedback of this method forces the detection. It must be considered that the detection levels have been established at ± 1 Hz according to IEC 61727 [10]. From Figs. 10(a) and 11(a), this method increases the measured ITHD due to a higher instability caused by the positive frequency feedback [21]. In case of harmonically distorted grid voltages, f_{DG} is 48–52 Hz during the grid-connected operation due to the control characteristics of the employed SPLL. Diverse approaches can be applied for the weakening of f_{DG}; however, as consequence, the detection times and the overall complexity would increase, i.e., adding specifically designed algorithms for frequency measurement. From Fig. 11(b), in the grid-connected operation, the ITHD increases due to the inherent instability of this method. From previous sections, the inner structure of the proposed wavelet-based method, i.e., decomposition level for detection purposes, does not depend on the PCC conditions which are only considered for the selection of the most suitable detection levels (Fig. 8). Moreover, the system stability is not affected by the proposed method.

IV. Experimental Results

The proposed detection technique has been tested using an experimental setup where two controllable dc sources *SM400* from Delta Elektronika substitute the PV array and, as H-bridge, has been employed an ac motor drive *VLT-5006* from Danfoss, which has been modified by disabling the rectification stage and including a custom interface and protection card developed by Aalborg University (Denmark). Due to the fact that the drive is 3ϕ, one leg of the IGBT bridge remains stopped during the developed islanding tests. The PV system controller, which includes the proposed wavelet-based approach, is executed on a $DS-1104$ control board from dSpace. The controller measures the inverter dc and grid voltages and the inverter output current, which flow through the LCL filter, in order to determine the inverter switching status. An isolation transformer is connected between the electrical grid and the PV inverter. The PV system provides $P = 529$ W to the local load. The islanding condition can be generated by disconnecting the grid side of the isolation transformer, which can be done by means of an available switch. Due to the characteristics of the developed setup, an LPF has been applied in order to smooth the c_5^p values and, as a consequence, T^{L} has been changed to 770.[Q] Three islanding tests have been carried out in order to evaluate the performance of the proposed controller under diverse operation conditions, namely, distorted grid voltage, frequency variations, and undervoltages.

Fig. 12 shows the obtained results in case of harmonically distorted grid voltages, based on the limits in IEEE Std. 519 (first, 100%; third, 2%; fifth, 2%; and seventh, 4%), the measured VTHD is 4.89. Channel 1 shows the distorted grid voltage during the tests, with high fifth and seventh voltage harmonics. Once the islanding condition occurs at 0.2 s, the proposed method stops the PV inverter in less than one cycle at the fundamental grid frequency, as shown in channels 3, A, and 2. The output current, shown in channel 4, also drops to zero after the islanding condition.

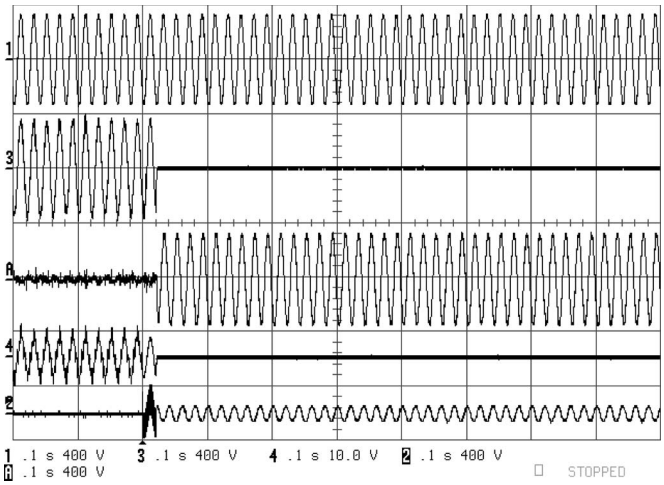

Fig. 12. Grid-disconnection transient in case of harmonically distorted grid voltage. Channel 1 is the measured grid voltage (400 V/div). Channel 3 is the PCC voltage (400 V/div). Channel A shows the difference between channels 1 and 3 (400 V/div). Channel 4 is the inverter output current (5 A/div). Channel 2 shows the voltage across the switch which disconnects the isolation transformer.

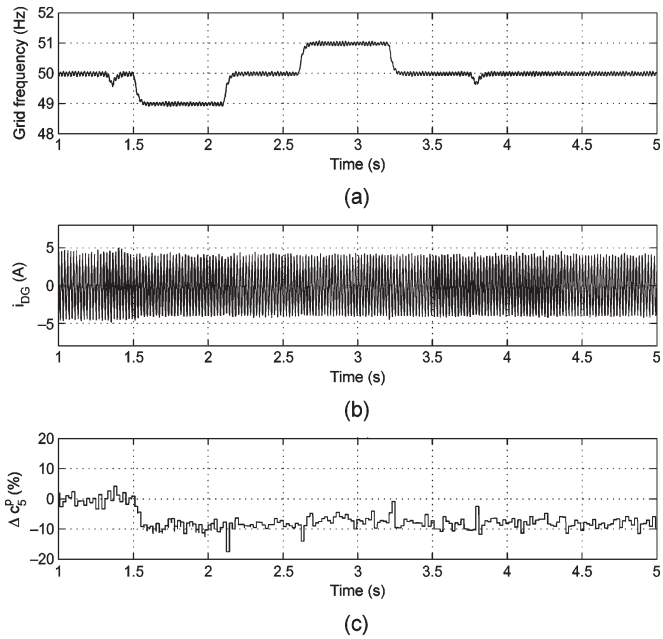

Fig. 13. Experimental tolerance test to frequency variations. (a) Applied frequency variation. (b) Measured output current. (c) Variation of c_5^p during the test.

A programmable power source has been employed in order to test the tolerance of the proposed method to grid frequency and voltage variations. The inner control variable Δc_5^p has been measured by means of the *ControlDesk* software, which is from dSpace. Fig. 13(a) shows the measured frequency during the first test; as can be seen, ± 1-Hz frequency steps are applied during 25 cycles at the fundamental grid frequency. The measured output current is shown in Fig. 13(b). The SPLL, employed as a grid synchronization mechanism, changes the frequency

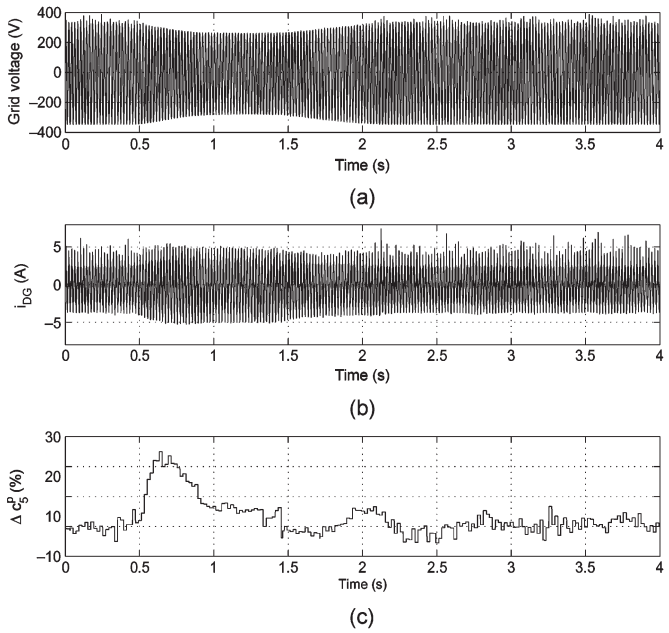

Fig. 14. Experimental tolerance test to voltage variations. (a) Applied voltage variation. (b) Measured output current. (c) Variation of c_5^p during the test.

of the PV inverter reference current, and the current controller tries to maintain the sinusoidal output current (during this test, the resonance frequency of the current controller shown in Fig. 1 is changed dynamically, considering the SPLL output). As can be seen, the current waveform remains almost the same. The measured relative variations of c_5^p in Fig. 13(c) show a correspondence between the output current waveform and Δc_5^p; however, the average value of Δc_5^p after the frequency step is -6.74%, which is not sufficient to trip the inverter.

The results of the voltage variations test are shown in Fig. 14. As shown in Fig. 14(a), the amplitude of the applied grid voltage drops to 25% during the test. In order to maintain the output power during the transient, the PV inverter generates an output current with a higher magnitude [Fig. 14(b)]. Due to the falling transient, Δc_5^p reaches a 24% value, which could trip the PV inverter in case of very adjusted detection levels due to the dynamics of the applied overall controller. The second transient is slower, and as a consequence, the measured variation is lower, reaching 6%.

V. Conclusion

This paper proposed a hybrid detection method which can detect the islanding condition from local measurements of PCC voltage and current signals, which are the basis of passive methods, but employed the high-frequency components injected by PV inverters due to the applied pulsewidth modulator, LCL filter, and current controller to reveal the islanding condition. The proposed method took advantage of the time and frequency localization of the DWT applied to the high-frequency components introduced by the DPGS inverter at the PCC. A theoretical analysis, the complete design process, and the obtained results, both in simulation and in experimental conditions, have been given in this paper. The proposed method, which has been validated in the presence of distorted grid voltages, frequency variations, and undervoltages, is suitable for low-voltage low-power PV systems, where a reduced number of sensors is available and the computational burden and complexity of the antiislanding algorithm must be minimized.

References

[1] J. M. Carrasco, L. G. Franquelo, J. T. Bialasiewicz, E. Galván, R. C. Portillo Guisado, M. A. M. Prats, J. I. Leon, and N. Moreno-Alfonso, "Power-electronic systems for the grid integration of renewable energy sources: A survey," *IEEE Trans. Ind. Electron.*, vol. 53, no. 4, pp. 1002–1016, Jun. 2006.

[2] F. Blaabjerg, R. Teodorescu, M. Liserre, and A. V. Timbus, "Overview of control and grid synchronization for distributed power generation systems," *IEEE Trans. Ind. Electron.*, vol. 53, no. 5, pp. 1398–1409, Oct. 2006.

[3] A. Kotsopoulos, P. J. M. Heskes, and M. J. Jansen, "Zero-crossing distortion in grid-connected PV inverters," *IEEE Trans. Ind. Electron.*, vol. 52, no. 2, pp. 558–565, Apr. 2005.

[4] G. Petrone, G. Spaguolo, R. Teodorescu, M. Veerachary, and M. Vitelli, "Reliability issues in photovoltaic power processing systems," *IEEE Trans. Ind. Electron.*, vol. 55, no. 7, pp. 2569–2580, Jul. 2008.

[5] G. M. Martins, J. A. Pomilio, S. Buso, and G. Spiazzi, "Three-phase low-frequency commutation inverter for renewable energy systems," *IEEE Trans. Ind. Electron.*, vol. 53, no. 5, pp. 1522–1528, Oct. 2006.

[6] A. Alepuz, S. Busquets-Monge, J. Bordonau, J. Gago, D. González, and J. Balcells, "Interfacing renewable energy sources to the utility grid using a three-level inverter," *IEEE Trans. Ind. Electron.*, vol. 53, no. 5, pp. 1504–1511, Oct. 2006.

[7] H. Ertl, J. W. Kolar, and F. C. Zach, "A novel multicell DC–AC converter for applications in renewable energy systems," *IEEE Trans. Ind. Electron.*, vol. 49, no. 5, pp. 1048–1057, Oct. 2002.

[8] H. Koizumi, T. Mizuno, T. Kaito, Y. Noda, N. Goshima, M. Kawasaki, K. Nagasaka, and K. Kurokawa, "A novel microcontroller for grid-connected photovoltaic systems," *IEEE Trans. Ind. Electron.*, vol. 53, no. 6, pp. 1889–1897, Dec. 2006.

[9] *IEEE Recommended Practice for Utility Interface of Photovoltaic (PV) Systems*, IEEE Std. 929-2000, 2000.

[10] *Photovoltaic (PV) Systems—Characteristics of the Utility Interface*, IEC 61727 Draft, Dec. 1, 2004.

[11] *Testing Procedure of Islanding Prevention Measures for Utility Interactive Photovoltaic Inverters*, IEC 62116, Jul. 2005.

[12] *Konzentrator-Photovoltaik (CPV)-Module und -Anordnungen Bauarteignung und Bauartzulassung (IEC 82/429/CDV:2006)*, Standard VDE 0126-33, 2006. Deutsche Fassung prEN 62108:2006.

[13] *IEEE Standard for Interconnecting Distributed Resources With Electric Power Systems*, IEEE Std. 1547-2003, Jul. 2003.

[14] *IEEE Standard Conformance Test Procedures for Equipment Interconnecting Distributed Resources With Electric Power Systems*, IEEE Std. 1547.1-2005, Jul. 2005.

[15] *IEEE Draft Application Guide for IEEE Standard 1547, Interconnecting Distributed Resources With Electric Power Systems*, IEEE P1547.2/D10, Mar. 2008.

[16] *IEEE Guide for Monitoring, Information Exchange, and Control of Distributed Resources Interconnected With Electric Power Systems*, IEEE 1547.3, Nov. 2007.

[17] R. A. Walling and N. W. Miller, "Distributed generation islanding—Implications on power system dynamic performance," in *Proc. IEEE Power Eng. Soc. Summer Meeting*, Jul. 2002, vol. 1, pp. 92–96.

[18] M. E. Ropp, K. Aaker, J. Haigh, and N. Sabbah, "Using power line carrier communications to prevent islanding [of PV systems]," in *Proc. 28th IEEE Photovoltaic Spec. Conf.*, Sep. 15–22, 2000, pp. 1675–1678.

[19] S. Islam, A. Woyte, R. Belmans, P. Heskes, P. M. Rooij, and R. Hogedoorn, "Cost effective second generation AC-modules: Development and testing aspects," *Energy*, vol. 31, no. 12, pp. 1897–1920, Sep. 2006.

[20] J.-M. Kwon, K.-H. Nam, and B.-H. Kwon, "Photovoltaic power conditioning system with line connection," *IEEE Trans. Ind. Electron.*, vol. 53, no. 4, pp. 1048–1054, Jun. 2006.

[21] W. Bower and M. E. Ropp, "Evaluation of islanding detection methods for photovoltaic utility-interactive power systems," Int. Energy Agency, Paris, France, Tech. Rep. Task V IEA-PVPS T5-09: 2002, Mar. 2002.

[22] M. E. Ropp, M. Begovic, A. Rohatgi, G. A. Kern, R. H. Bonn, Sr., and S. Gonzalez, "Determining the relative effectiveness of islanding detection methods using phase criteria and nondetection zones," *IEEE Trans. Energy Convers.*, vol. 15, no. 3, pp. 290–296, Sep. 2000.

[23] K. El-Arroudi, G. Joós, I. Kamwa, and D. T. McGillis, "Intelligent-based approach to islanding detection in distributed generation," *IEEE Trans. Power Del.*, vol. 22, no. 2, pp. 828–835, Apr. 2007.
[24] C. Jeraputra and P. N. Enjeti, "Development of a robust anti-islanding algorithm for utility interconnection distributed fuel cell powered generation," *IEEE Trans. Power Electron.*, vol. 19, no. 5, pp. 1163–1170, Sep. 2004.
[25] M. Liserre, A. Pigazo, A. Dell'Aquila, and V. M. Moreno, "An anti-islanding method for single-phase inverters based on a grid voltage sensorless control," *IEEE Trans. Ind. Electron.*, vol. 53, no. 5, pp. 1418–1426, Oct. 2006.
[26] Z. Ye, A. Kolwalkar, Y. Zhang, P. Du, and R. Walling, "Evaluation of anti-islanding schemes based on nondetection zone concept," *IEEE Trans. Power Electron.*, vol. 19, no. 5, pp. 1171–1176, Sep. 2004.
[27] H. H. Zeineldin, E. F. El-Saadany, and M. M. A. Salama, "Impact of DG interface control on islanding detection and nondetection zones," *IEEE Trans. Power Del.*, vol. 21, no. 3, pp. 1515–1523, Jul. 2006.
[28] F. De Mango, M. Liserre, and A. Dell'Aquila, "Overview of anti-islanding algorithms for PV systems. Part II: Active methods," in *Proc. 12th Int. EPE-PEMC*, Aug. 30–Sep. 1, 2006, pp. 1884–1889.
[29] G.-K. Hung, C.-C. Chang, and C.-L. Chen, "Automatic phase-shift method for islanding detection of grid-connected photovoltaic inverters," *IEEE Trans. Energy Convers.*, vol. 18, no. 1, pp. 169–173, Mar. 2003.
[30] A. V. Timbus, R. Teodorescu, F. Blaabjerg, and U. Borup, "ENS detection algorithm and its implementation for PV inverters," *Proc. Inst. Electr. Eng.—Electric Power Applications*, vol. 153, no. 2, pp. 206–212, Mar. 2006.
[31] C. Hernández González and R. Iravani, "Current injection for active islanding detection of electronically-interfaced distributed resources," *IEEE Trans. Power Del.*, vol. 21, no. 3, pp. 1698–1705, Jul. 2006.
[32] L. Asiminoaei, R. Teodorescu, F. Blaabjerg, and U. Borup, "Implementation and test of an online embedded grid impedance estimation technique for PV inverters," *IEEE Trans. Ind. Electron.*, vol. 52, no. 4, pp. 1136–1144, Aug. 2005.
[33] B. Yu, Y. Jung, J. So, H. Hwang, and G. Yu, "A robust anti-islanding method for grid-connected photovoltaic inverter," in *Proc. 4th IEEE World Conf. Photovoltaic Energy Convers.*, May 2006, pp. 2242–2245.
[34] J. B. Jeong and H. J. Kim, "Active anti-islanding method for PV system using reactive power control," *Electron. Lett.*, vol. 42, no. 17, pp. 1004–1005, Aug. 2006.
[35] L. A. C. Lopes and H. Sun, "Performance assessment of active frequency drifting islanding detection methods," *IEEE Trans. Energy Convers.*, vol. 21, no. 1, pp. 171–180, Mar. 2006.
[36] H. H. Zeineldin, E. F. El-Saadany, and M. M. A. Salama, "Islanding detection of inverter-based distributed generation," *Proc. Inst. Electr. Eng.—Generation Transmission Distribution*, vol. 153, no. 6, pp. 644–652, Nov. 2006.
[37] J. Yin, L. Chang, and C. Diduch, "A new hybrid anti-islanding algorithm in grid connected three-phase inverter system," in *Proc. 37th IEEE Power Electron. Spec. Conf.*, Jun. 2006, pp. 1–7.
[38] A. Pigazo, V. M. Moreno, M. Liserre, and A. Dell'Aquila, "Wavelet-based islanding detection algorithm for single-phase photovoltaic (PV) distributed generation systems," in *Proc. IEEE Int. Symp. Ind. Electron.*, Jun. 2007, pp. 2409–2413.
[39] N. Femia, D. Granozio, G. Petrone, G. Spagnuolo, and M. Vitelli, "Predictive & adaptive MPPT perturb and observe method," *IEEE Trans. Aerosp. Electron. Syst.*, vol. 43, no. 3, pp. 934–950, Jul. 2007.
[40] M. Liserre, R. Teodorescu, and F. Blaabjerg, "Stability of grid-connected PV inverters with large grid impedance variation," in *Proc. IEEE 35th Annu. Power Electron. Spec. Conf.*, Jun. 2004, vol. 6, pp. 4773–4779.
[41] R. Teodorescu, F. Blaabjerg, M. Liserre, and P. C. Loh, "Proportional-resonant controllers and filters for grid-connected voltage-source converters," *Proc. Inst. Electr. Eng.—Electric Power Applications*, vol. 153, no. 5, pp. 750–762, Sep. 2006.
[42] D. G. Holmes and T. A. Lipo, *Pulse Width Modulation for Power Converters. Principles and Practice*. Piscataway, NJ: IEEE Press, 2003.
[43] V. A. Katic, J. M. Knezevic, and D. Graovac, "Application-oriented comparison of the methods for AC/DC converter harmonics analysis," *IEEE Trans. Ind. Electron.*, vol. 50, no. 6, pp. 1100–1108, Dec. 2003.
[44] E. F. El-Saadany, T. K. Abdel-Galil, and M. M. A. Salama, "Application of wavelet transform for assessing power quality in medium voltage industrial distribution system," in *Proc. IEEE/PES Transmiss. Distrib. Conf. Expo.*, Oct. 28–Nov. 2, 2001, vol. 1, pp. 427–432.
[45] S. Mallat, *A Wavelet Tour of Signal Processing*, 2nd ed. San Diego, CA: Academic, 1999.
[46] G. Strang and T. Nguyen, *Wavelets and Filter Banks*, 2nd ed. Wellesley, MA: Wellesley College, 1996.

Alberto Pigazo (M'05) received the M.Sc. and Ph.D. degrees in physics (electronics) from the University of Cantabria, Santander, Spain, in 1997 and 2004, respectively.

He was a Visiting Researcher and Professor with the Politecnico di Bari, Bari, Italy. Since October 2000, he has been with the Department of Electronics and Computers, University of Cantabria, where he is currently an Assistant Professor teaching courses in electronics, power electronics, and digital signal processing. His main research interests include electrical power quality and digital signal-processing techniques applied to the control of power converters.

Dr. Pigazo is member of the IEEE Industrial Electronics Society (IES), the Editorial Board of IEEE Industrial Electronics Magazine (IEM), and the IES Technical Committee on Renewable Energy Systems. As an author and Reviewer, he has been contributing for IEEE conferences and journals.

Marco Liserre (S'00–M'02–SM'07) received the M.Sc. and Ph.D. degrees in electrical engineering from the Politecnico di Bari, Bari, Italy, in 1998 and 2002, respectively.

Since January 2004, he has been an Assistant Professor with the Politecnico di Bari, where he is engaged in teaching courses of power electronics, industrial electronics, and electrical machines. He has authored or coauthored more than 127 technical papers, 28 of them published or to be published in international peer-reviewed journals, and three chapters of a book. These works have received more than 800 citations. He has been a visiting Professor at Aalborg University, Denmark, Alcala de Henares, Spain, and at Christian-Albrechts University of Kiel, Germany. His current research interests include industrial electronics applications to distributed power generation systems based on renewable energies.

Dr. Liserre is a Senior Member of the following IEEE societies: Industrial Electronics Society (IES), Power Electronics Society, and Industry Applications Society. He was a Reviewer for international conferences and journals. Within the IES, he has been responsible for student activities, an AdCom member, an Editor of the newsletter, and responsible for region 8 membership activities. He has been involved in the IEEE conferences organization in different capacities. He is an Associate Editor of the IEEE TRANSACTIONS ON INDUSTRIAL ELECTRONICS. He is the Founder and the Editor-in-Chief of the *IEEE Industrial Electronics Magazine* 2007–2009. He is the Founder and the Chairman of the Technical Committee on Renewable Energy Systems of the IEEE Industrial Electronics Society. He has been a Guest Co-Editor-in-Chief of the IEEE TRANSACTIONS ON INDUSTRIAL ELECTRONICS for the Special Section "Voltage and current control of power converters." He is also an Organizer and a Guest Co-Editor-in-Chief of the new Special Section on "Renewable Energy Systems" of the IEEE TRANSACTIONS ON INDUSTRIAL ELECTRONICS. He has received the IES 2009 Early Career Award. He will be the Co-Chairman of the International Symposium on Industrial Electronics (ISIE 2010), that will be held in Bari 4–7 July 2010. He has been giving lectures at different universities and tutorials for the following conferences: IEEE Energy Conversion Congress and Exposition (ECCE) 2009, IEEE Power Electronics Specialists Conference (PESC) 2008, International Symposium on Industrial Electronics (ISIE) 2008, European Conference on Power Electronics and Applications (EPE) 2007, Annual Conference of the IEEE Industrial Electronics Society (IECON) 2006, ISIE 2006, and IECON 2005.

Rosa A. Mastromauro (S'05–M'09) received the M.Sc. and Ph.D. degrees in electrical engineering from the Politecnico di Bari, Bari, Italy, in 2005 and 2009, respectively.

Since 2005, she has been with the Converters, Electrical Machines and Drives Research Team, Politecnico di Bari where she is engaged in teaching course of power electronics. Her research interests include power converter control for distributed power generation systems based on renewable energies.

Dr. Mastromauro is a member of the IEEE Industrial Electronics Society, IEEE Power Electronics Society, IEEE Industrial Application Society and IEEE Women in Engineering Society, and Italian Electrotechnical and Electronic Association. She is a reviewer for IEEE conference proceedings and journals.

Víctor M. Moreno (M'01) received the M.Sc. and Ph.D. in physics (electronics) from the University of Cantabria, Santander, Spain, in 1980 and 1994, respectively.

He is currently an Associate Professor with the Department of Electronics and Computers, University of Cantabria. His research interests include electrical power quality, electromagnetic compatibility, digital signal processing, and digital control of power converters.

Dr. Moreno is a member of the IEEE Power Electronics Society (PELS). He was a recipient of the Viesgo Award, in 1994, for his Ph.D. thesis, entitled *Distributed System for the Measurement and Analysis of Electrical Power Quality Applying Kalman Filtering*. He has been collaborating for IEEE journals as a Reviewer.

Antonio Dell'Aquila (M'87) received the M.Sc. degree in electrical engineering from the Università degli Studi di Bari, Bari, Italy, in 1970.

Since 1970, he has been with the Converters, Electrical Machines, and Drives Research Team, Politecnico di Bari, Bari, where he is currently a Full Professor of electrical machines, power electronics, and electrical drives with the Department of Electrical and Electronics Engineering. He has published more than 100 technical papers on electrical machine models; transient analysis of rotating machines; inverter-fed induction machine performance; digital signal processing for nonsinusoidal waveforms; Kalman filtering for real-time estimation of induction motor parameters; and control, monitoring, and diagnostics of ac drives. His research interests include harmonic pollution produced by electronic power systems, pulsewidth modulation techniques for power converters, power converters in renewable energy conversion systems, active power filters, multilevel inverters, and intelligent control of power electronics equipment with fuzzy logic controllers.

Dr. Dell'Aquila is a member of the IEEE Power Engineering Society and the Italian Electrotechnical and Electronic Association. He is Dean of the Faculty of Engineering, Politecnico di Bari, Italy.